A&A 508, 1045–1056 (2009)
DOI: 10.1051/0004-6361/200811462

Astronomy & Astrophysics

Properties of the nuclei and comae of 13 ecliptic comets from Hubble Space Telescope snapshot observations

P. L. Lamy[1], I. Toth[1,2], H. A. Weaver[3], M. F. A'Hearn[4], and L. Jorda[1]

[1] Laboratoire d'Astrophysique de Marseille, UMR6110 CNRS/Université de Provence, 38 rue Frédéric Joliot-Curie, 13388 Marseille Cedex 13, France
e-mail: philippe.lamy@oamp.fr
[2] Konkoly Observatory, Budapest 1525, PO Box 67, Hungary
[3] Applied Physics Laboratory, The Johns Hopkins University, Laurel, MD 20723-6099, USA
[4] Department of Astronomy, University of Maryland, College Park, MD 20742, USA⋆

Received 2 December 2008 / Accepted 13 October 2009

ABSTRACT

Context. Knowledge of the size distribution of cometary nuclei and, more generally, of their physical properties is important for constraining models of the formation and evolution of the Solar System.
Aims. We report on our on-going effort to determine the ensemble properties of comets based on our success in detecting the nuclei of active comets with the Hubble Space Telescope (HST).
Methods. During cycle 8 (July 1999 to June 2000), we observed 13 ecliptic comets with the planetary camera 2 through at least two filters (V and R) and up to four (B, V, R, I) for the brightest ones. The ∼30 min of HST observational time devoted to each comet did not permit a proper determination of light curves, so our "snapshot" observations yield effective radii, not shapes.
Results. Assuming spherical nuclei with a geometric albedo of 0.04 for the R band (except 0.024 for 10P/Tempel 2, as independently measured) and a phase law of 0.04 mag/deg, we obtained the following effective radii: 4P/Faye: 1.77 km, 10P/Tempel 2: 5.98 km, 17P/Holmes: 1.71 km, 37P/Forbes: 0.81 km 44P/Reinmuth 2: 1.61 km, 50P/Arend: 0.95 km, 59P/Kearns–Kwee: 0.79 km, 63P/Wild 1: 1.46 km, 71P/Clark: 0.68 km, 84P/Giclas: 0.90 km, 106P/Schuster: 0.94 km, 112P/Urata–Niijima: 0.90 km, 114P/Wiseman–Skiff: 0.78 km. In our present sample, eight out of thirteen nuclei have sub-kilometer radii. The average color of the observed nuclei is $(V - R) = 0.52 \pm 0.04$, which is significantly redder than the Sun. We determined the dust activity parameter $Af\rho$ of their coma in the R band, and estimated the dust production rates. The average reflectivity gradient of the dust comae of six comets is $S'[670, 792\ \mathrm{nm}] = 15.2 \pm 2.3\%$ per kÅ.

Key words. comets: general – methods: data analysis – techniques: photometric – techniques: image processing – telescopes – solar system: general

1. Introduction

Knowledge of the size distribution of cometary nuclei and, more generally, of their physical properties, is important for constraining models of the formation and evolution of the Solar System. Based on our initial success in detecting the nuclei of *active* comets with the Hubble space telescope (HST), we started a program to determine their ensemble properties. We recall that our basic approach takes advantage of the high spatial resolution of the planetary camera (WFPC2) mode of the HST, 0.″0455 pixel^{-1}, to "photometrically resolve" the nucleus in the presence of a surrounding coma. We refer the reader to our review article (Lamy et al. 2004), and references therein, for an overview of our past work and results. We present below the detailed analysis of the snapshot observations performed during cycle 8 of the HST (July 1999 to June 2000). We selected 13 short-period comets that came reasonably close to Earth during cycle 8 to maximize the spatial resolution and, thus, the contrast between the nucleus and the coma. The principal orbital parameters of the observed comets are given in Table 1.

The nuclei of all 13 comets were detected, and we determined their radii (assuming an albedo and a phase function) and their colors. Their comae were also characterized by their $Af\rho$ values, which are proportional to the dust production rate and the dust reflectivity.

2. Observations and data analysis

The journal of the observations, as well as the geometric circumstances, are presented in Table 2. A single HST orbit, which has ∼30 min of observing time available (including overhead), was devoted to each of the 13 comets. All the comets were observed with the planetary camera (PC) mode of the WFPC2 and with the broadband F675W and F555W filters. When the exposure times were short, we could add observations with the F439W and F814W filters. Table 3 gives the characteristics of these filters (Biretta et al. 1996). The pixel scale of 0.045 arcsec translated to a typical projected distance at the comets of ∼50 km with extreme values of 25.8 km (106P) and 71.8 km (17P). All images were processed using the routine science data processing system at the Space Telescope Science Institute. Figure 1 illustrates one of the F675W images for each comet.

For the analysis of the data, we applied our standard method of fitting a parametric model of the expected surface brightness

⋆ Based on observations made with the NASA/ESA Hubble space telescope, obtained at Space Telescope Science Institute, which is operated by the Association of Universities for Research in Astronomy under NASA contract NAS 5-26555.

Table 1. Orbital elements of the comets.

Comet	q (AU)	Q (AU)	e	i (°)
4P/Faye	1.65	6.02	0.56	9.0
10P/Tempel 2	1.48	4.72	0.52	11.9
17P/Holmes	2.16	5.21	0.41	19.1
37P/Forbes	1.44	5.26	0.56	7.1
44P/Reinmuth 2	1.89	5.23	0.46	7.0
50P/Arend	1.85	6.24	0.53	19.9
59P/Kearns–Kwee	2.33	6.60	0.47	9.3
63P/Wild 1	1.98	9.24	0.64	19.9
71P/Clark	1.55	4.68	0.50	9.5
84P/Giclas	1.84	5.44	0.49	7.2
106P/Schuster	1.62	5.97	0.57	20.1
112P/Urata–Niijima	1.44	5.61	0.58	24.2
114P/Wiseman–Skiff	1.56	5.51	0.56	18.2

q: perihelion distance.
Q: aphelion distance.
e: eccentricity.
i: inclination.

to the observed images. The most general model, represented by a 2-dimensional array of brightness values, is simply given by

$$\text{Model} = [\text{nucleus} + \text{coma}] \otimes \text{PSF} \quad (1)$$

where PSF denotes the point spread function of the telescope and $\otimes$ represents the convolution operator. The nucleus is not resolved so that

$$\text{nucleus} = k_{\rm n}\, \delta(\rho) \quad (2)$$

where δ is the Dirac's delta function, ρ is the radial distance from the center, and $k_{\rm n}$ is a scaling factor. Specifying a model for the coma very much depends on how complex it appears on the actual images, and we developed various models accordingly in our past work (Lamy et al. 2004). As expected, most of the comae are circularly symmetric, and the few exceptions do not sufficiently depart from this property to warrant the most general procedure we implemented for comet Hale-Bopp (Weaver & Lamy 1999). We therefore use the simple isotropic model

$$\text{coma} = k_{\rm c}\ \rho^{p} \quad (3)$$

where $k_{\rm c}$ is a scaling factor for the coma, and p is the power exponent of the brightness variation versus distance from the nucleus (optocenter) in the image plane. The point spread function (PSF) of the telescope was modeled using version 4.0 b of the TinyTIM software written by Krist (1995) which has the capability of including the jitter of the HST, sometime conspicuous on long exposures. To account for the sub-pixel location of the nucleus, which may cause a marked asymmetry of the brightness profiles, the model images were generated on a finer grid than the original PC pixel, with a sub-sampling factor of 9. The fit to the real images was performed after integrating the model over 9×9 sub-pixels to recover the original pixel of the PC. Note that the ρ^p function was rigorously calculated in the central 3×3 pixels to account for the finite extent of the pixels; this effect is negligible beyond this central area.

The sub-pixel locations of the nuclei (x_n, y_n) were first determined using the X and Y-profiles through the pixels displaying the peak signals, and using initial estimates for the model parameters $k_{\rm n}$, $k_{\rm c}$ and p. Their final determinations, as well as those of the jitter if any, were performed on azimuthally averaged radial profiles as introduced in the case of comet 46P/Wirtanen (Lamy et al. 1998a). This is implemented straightforwardly by performing a polar transformation of the images centered on the nucleus (the pixel having the largest signal) with an angular resolution of 1° and summing the 360 individual profiles. All coma profiles were fitted using the canonical value $p = -1$ except for those of 50P/Arend and 71P/Clark, as will be discussed later.

The 1σ error affecting the data can be expressed as

$$s = \sqrt{\frac{B}{g} + \left(\frac{\Re}{g}\right)^2 + (fB)^2} \quad (4)$$

where B is the observed signal in DN, $g = 7$ electrons DN^{-1} is the gain, $\Re = 5$ electrons is the readout noise, and $f = 0.01$ expresses the flat field noise as a fraction of the signal. The azimuthal averaging of the 360 profiles reduces the error, typically by $\sqrt{360}$, although strictly speaking, the profiles are not uncorrelated. The error from the fitting procedure is expressed as a fraction of the signal in the peak pixels, where the signal is dominated by the nucleus

$$\sigma_f = \varepsilon_f B \quad (5)$$

where ε_f is estimated from the residuals and typically ranges from 0.02 to 0.05. The 1σ error in the signal of the nucleus is therefore given by

$$\sigma^2 = \frac{s^2}{360} + \varepsilon_f^2 B^2 \quad (6)$$

and is always dominated by the second term, i.e., the error from the fitting procedure.

The determination of the absolute magnitudes was performed on the k_nPSF images, which measure the brightness of the nucleus as it would be observed by the HST in the absence of coma. The procedure followed the recommendations of Holtzman et al. (1995). The so-called instrumental magnitudes were calculated by integrating the scaled PSFs in an aperture of 0.5″ radius, so that no aperture correction is required. The formulae converting the instrumental WFPC2 magnitudes to the standard Johnson-Kron-Cousins R magnitudes require a color correction in first and second orders, of the $(V - R)$ color index. Since we always have observations in at least two filters, we could combine the formulae and solved for all magnitudes without any assumption for the color of the nucleus. The errors σ affecting the signal of the nucleus (Eq. (6)) were propagated through the transformation formulae and the final uncertainties on the R magnitudes listed in Table 4 include the systematic errors in the zero-points of the calibration.

3. The properties of the nuclei

The apparent R magnitude of a body is related to its physical properties by (Russell 1916; Keller 1990; Jewitt 1991):

$$p_R\, \phi(\alpha) r_{\rm n}^2 = 2.238 \times 10^{22} r_{\rm h}^2 \Delta^2 10^{0.4(R_{\rm Sun} - R_{\rm Nuc})} \quad (7)$$

p_R is the geometric albedo in the R band, $\phi(\alpha)$ is the phase function at phase angle α (deg) in the same band, $r_{\rm n}$ is the nucleus radius (m); $r_{\rm h}$, Δ are the heliocentric and geocentric distances (AU); $R_{\rm Sun}$ is the apparent R magnitude of the Sun, and $R_{\rm Nuc}$ is the apparent R magnitude of the nucleus. We assume $p_R = 0.04$ and $\phi(\alpha) = 10^{-0.4\alpha\beta}$ with a phase coefficient $\beta = 0.04$ mag/deg, as used in our previous work. Note that, whenever possible, we imposed among our observational constraints that the nuclei be observed at $\alpha > 5°$ so as to avoid a

Table 2. Journal of the observations.

Comet	Date (UT)	Filters	r_h (AU)	Δ (AU)	α (°)	Scale (km/pix)
4P/Faye	2000 Feb. 07.618	*V*, *R*	2.956	1.998	5.6	66.0
10P/Tempel 2	1999 Jun. 23.432	*B*, *V*, *R*, *I*	1.669	0.681	12.8	22.5
17P/Holmes	1999 Jun. 15.527	*V*, *R*	3.116	2.176	8.5	71.8
37P/Forbes	1999 Oct. 29.326	*V*, *R*, *I*	2.270	1.389	14.8	45.8
44P/Reinmuth 2	2000 Jun. 12.638	*V*, *R*	2.727	1.732	5.3	57.2
50P/Arend	2000 Jan. 11.854	*V*, *R*, *I*	2.374	1.468	11.8	48.4
59P/Kearns–Kwee	2000 Jan. 15.542	*V*, *R*, *I*	2.516	1.539	3.3	50.8
63P/Wild 1	2000 Apr. 22.212	*V*, *R*, *I*	2.266	1.299	9.2	42.9
71P/Clark	2000 Mar. 12.701	*V*, *R*	2.715	1.764	7.5	58.2
84P/Giclas	2000 Jan. 13.444	*V*, *R*	2.209	1.368	16.9	45.2
106P/Schuster	1999 Oct. 18.708	*B*, *V*, *R*, *I*	1.666	0.780	23.0	25.8
112P/Urata–Niijima	1999 Sep. 08.618	*V*, *R*	2.296	1.501	19.2	49.5
114P/Wiseman–Skiff	2000 Jan. 14.444	*B*, *V*, *R*, *I*	1.569	0.836	33.2	27.6

Date: mid-point of the observational session (visit) bracketed by the first and last images (UT).
Filters: (*B*, *V*, *R*, *I*) = (F439W, F555W, F675W, F814W).
r_h: heliocentric discance, Δ: geocentric discance, α: solar phase angle.
Scale: pixel scale at the nucleus distance.

Table 3. Characteristics of the filters.

Name	$\overline{\lambda}$	$\Delta\lambda$
F439W	423	47
F555W	540	123
F675W	670	89
F814W	792	149

$\overline{\lambda}$, the mean wavelength (nm).
$\Delta\lambda$, equivalent width (nm).
Definitions are given in Biretta et al. (1996).

possible opposition effect (whose representation would require two unknown parameters), which allows us to remain in the quasi-linear regime of the phase function (only one parameter needed: β). There is one exception, namely 59P, observed at $\alpha = 3.^\circ3$., and the possible implication will be discussed later.

We now present our results for the 13 nuclei detected with the HST from July 1999 to June 2000. The ~30 min of HST observing time devoted to each comet did not permit the determination of secure light curves, so our "snapshot" observations yield effective radii, not shapes. An effective radius $r_{n,a}$ is defined as that of a disk having the same instantaneous projected area as the observed nucleus and will range between $\sqrt{ab}$ and b for a spheroid of semiaxes a and $b = c$ with its spin axis along one of its short axes perpendicular to the direction to the Earth. As discussed by Lowry & Weissman (2003) and Lamy et al. (2004), a snapshot observation leads, on average, to an instantaneous projected area close to the maximum cross-section $\sqrt{\pi ab}$, and the effective radius $r_{n,a}$ gives, on average, an excellent estimate of the effective radius of the equivalent sphere $r_{n,v}$ defined by $r_{n,v}^3 = ab^2$. For each nucleus, we briefly summarize other determinations of its size based on the more extensive discussion provided in our review article (Lamy et al. 2004). Color indices are reported, but their interpretation in the general context of the primitive bodies in the solar system is presented elsewhere (Lamy & Toth 2009).

3.1. 4P/Faye

This comet was observed with the HST on 7 February 2000 at r_h = 2.96 AU outbound, Δ = 2.0 AU, and at a solar phase angle of 5.°6. The previous perihelion passage took place on 6 May 1999 at r_h = 1.6 AU. The coma was in steady state with $p = -1$. Its nucleus was easily detected with a good contrast in all images (see Fig. 2 for an example). The two F675W images yielded an average value of the nucleus radius of 1.77 ± 0.04 km. We obtained a color index $(V - R) = 0.45 \pm 0.04$.

4P/Faye is the first nucleus detected with the HST (WFPC1), in October–November 1991 (Lamy & Toth 1995; Lamy et al. 1996) during its first year of operation, when the comet was at

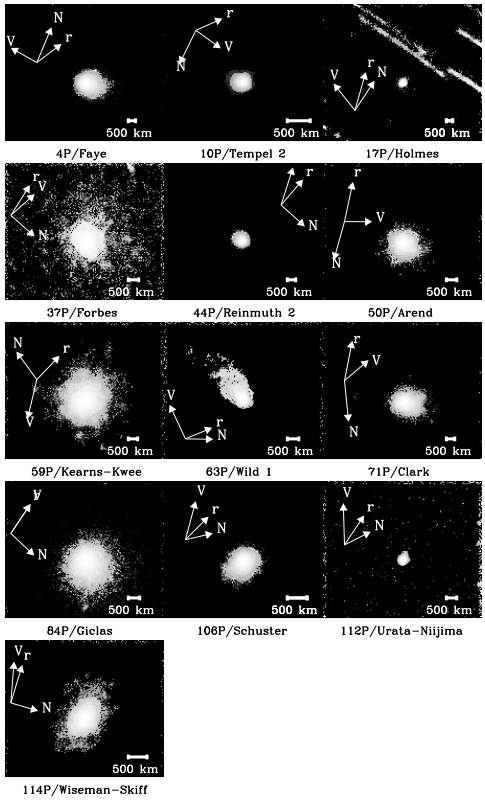

Fig. 1. Examples of the HST PC2 images of 13 comets taken with the *F675W* filter. Each square image is 170 × 170 pixels, that is 7.7×7.7 arcsec^2. The arrows indicate the anti-solar direction (prolonged radius vector $\boldsymbol{r}$), the direction of celestial north ($\boldsymbol{N}$), and the heliocentric orbital velocity vector ($\boldsymbol{V}_{orb}$) of the comet projected onto the sky plane.

Table 4. Properties of the nuclei of the comets.

Comet	R_{app} (mag)	r_n (km)	$(V-R)$	$(B-V)$	$(R-I)$
Solar colors:			0.35	0.65	0.28
4P/Faye	20.12 ± 0.03	1.77 ± 0.04	0.45 ± 0.04	–	–
10P/Tempel 2	14.77 ± 0.03	$5.98 \pm 0.04^*$	0.49 ± 0.03	0.80 ± 0.02	0.52 ± 0.03
17P/Holmes	20.61 ± 0.04	1.71 ± 0.07	0.56 ± 0.02	–	–
37P/Forbes	20.83 ± 0.04	0.81 ± 0.04	0.29 ± 0.03	–	0.66 ± 0.06
44P/Reinmuth 2	19.83 ± 0.05	1.61 ± 0.07	0.62 ± 0.08	–	–
50P/Arend	20.58 ± 0.04	0.95 ± 0.03	0.81 ± 0.10	–	0.26 ± 0.09
59P/Kearns–Kwee	20.86 ± 0.05	0.79 ± 0.03	0.62 ± 0.07	–	0.27 ± 0.08
63P/Wild 1	19.17 ± 0.02	1.46 ± 0.03	0.50 ± 0.05	–	0.42 ± 0.04
71P/Clark	21.83 ± 0.07	0.68 ± 0.04	0.64 ± 0.07	–	–
84P/Giclas	20.59 ± 0.04	0.90 ± 0.05	0.32 ± 0.03	–	–
106P/Schuster	18.91 ± 0.03	0.94 ± 0.03	0.52 ± 0.06	1.01 ± 0.06	0.45 ± 0.06
112P/Urata–Niijima	20.96 ± 0.04	0.90 ± 0.05	0.53 ± 0.04	–	–
114P/Wiseman–Skiff	19.73 ± 0.04	0.78 ± 0.05	0.46 ± 0.02	0.85 ± 0.03	0.54 ± 0.02

R_{app}: apparent magnitude of the nucleus in the Johnson–Kron–Cousins photometric system.
r_n: effective radius of the nucleus assuming $p_R = 0.04$, $\beta = 0.040$ mag/deg except 10P/Tempel 2 $(V-R)$, $(B-V)$, $(R-I)$: color indices.
*using $p_R = 0.024$ as measured independently.

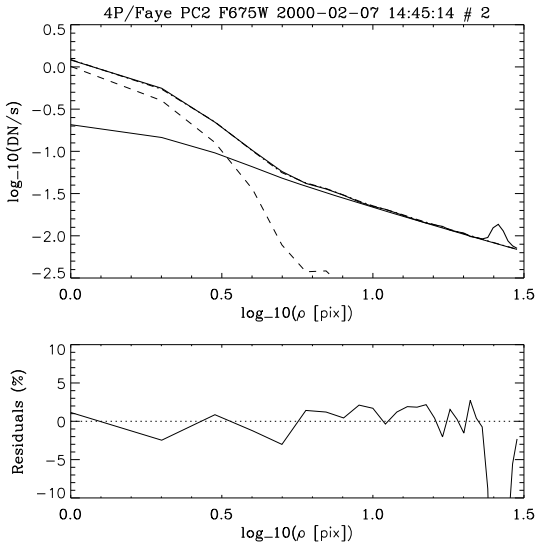

Fig. 2. Azimuthally averaged radial surface brightness profile of a F675W image of 4P/Faye in log−log representation (*top*). The thick solid line represents the observation, the dashed line is the estimated signal from the nucleus, the thin solid line is the estimated coma, and the dash-dot line is the fitted model. The graph (*bottom*) displays the residuals in percents.

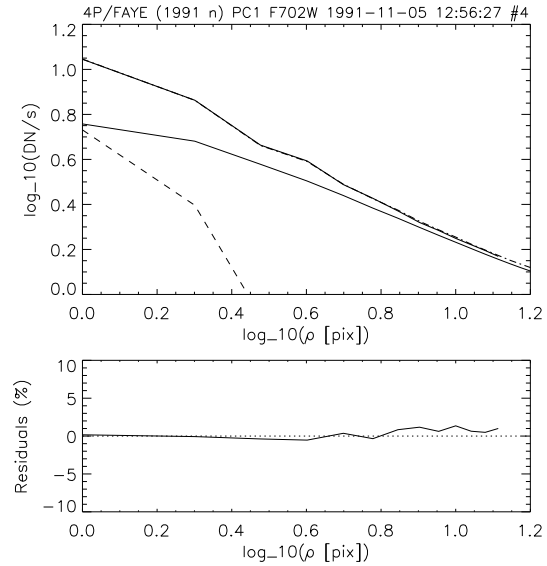

Fig. 3. Same as Fig. 2 but for a F702W image of 4P/Faye taken on 5.54 November 1991 with the aberrated HST and the first planetary camera (WFPC1).

$r_h = 1.6$ AU and $\Delta = 0.62$ AU. We then determined a larger size ranging from 2.34 to 2.9 km. Re-examination of the 1991 observations, obtained with the *aberrated* HST, indicated that the signal from the nucleus was overestimated. We decided to re-analyze these images owing to several major improvements that have been made possible during the past decade:

i) all images were re-processed at the Space Telescope Science Institute taking advantage of the experience accumulated on the instrument and of better calibrations;
ii) the model of the aberrated PSFs has significantly been refined in the subsequent releases of the TinyTIM program (Krist 1995);
iii) better understanding and procedures of images fitting were developed during our on-going analysis of HST cometary images.

Retrospectively, our early fits were not so satisfactory, and the models overshot the observed signals in the central pixels (see for instance Fig. 5 of Lamy et al. 1996), yielding sizes that were too large. Figure 3 gives an example of the much better fit we now achieve on the aberrated images. The corresponding values of the nuclear radius range from 1.38 to 1.45 km with an average of 1.4 km. This is ~20% less than our present value of 1.77 km. However, it is entirely possible that we were seeing two different cross-sections of a rotating, elongated body in 1991 and 2000. If πab and πb^2 denote the two extreme cross-sections, we find $a = 2.24$, $b = 1.4$ km and $a/b = 1.6$, a quite reasonable value but strictly speaking, a lower limit. Recently, Lowry & Weissman (2003) reported only an upper bound for the radius, $r_n \leq 18.4$ km based on the 3σ upper limit on the total R magnitude of the comet and assuming $p_R = 0.04$.

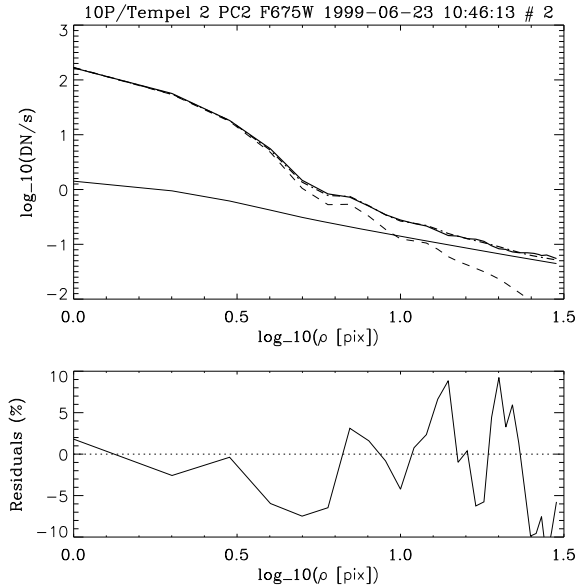

Fig. 4. Same as Fig. 2 for 10P/Tempel 2.

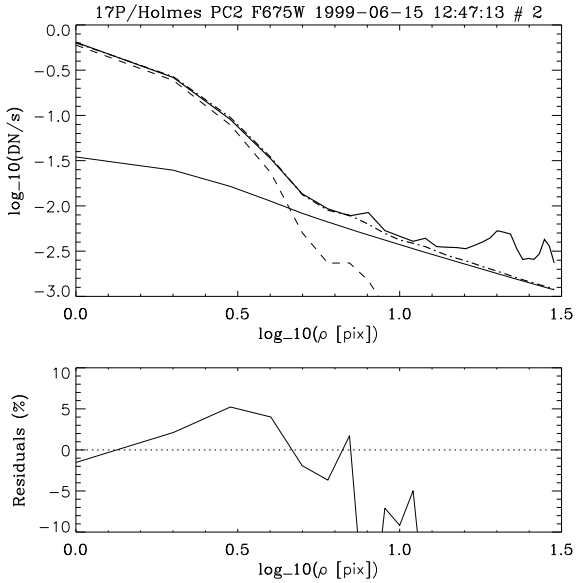

Fig. 5. Same as Fig. 2 for 17P/Holmes.

3.2. 10P/Tempel 2

10P was observed with the HST on 23 June 1999 when the comet was at $r_h = 1.67$ AU inbound, $\Delta = 0.68$ AU and at a solar phase angle of 12°.8. The comet later reached perihelion on 8 September 1999 at $r_h = 1.48$ AU. The coma was in steady state with $p = -1$. The signal is dominated by the nucleus with a negligible contribution from the coma in the central pixels ($\rho \leq 5$) as illustrated in Fig. 4. The four F675W images yielded an average value of the nucleus of 4.63 ± 0.03 km. We obtained color indices $(B - V) = 0.80 \pm 0.02$, $(V - R) = 0.49 \pm 0.03$ and $(R - I) = 0.52 \pm 0.03$.

Thanks to its faint coma, the nucleus of 10P was extensively observed from the ground namely by A'Hearn et al. (1989), who combined optical and infrared photometry, and by Jewitt & Luu (1989), who performed CCD photometry from aphelion (thus, convincingly detecting a bare nucleus) to perihelion. Their interpretations converge to a spheroidal nucleus with $a = 8-8.15$ km and $b = c = 4-4.3$ km with an albedo $p_R = 0.024 \pm 0.005$ and a rotational period of ~9 h. The effective radius from the equivalent cross-section is $r_{n,a} = 5.7-5.9$ km, while that from the equivalent volume is $r_{n,v} = 5.0-5.3$ km. If we scale our result to the above albedo $p_R = 0.024$, we obtain $r_n = 5.98 \pm 0.04$ km in agreement with the ground-based determination. This incidentally confirms the point emphasized by Lowry & Weissman (2003) and Lamy et al. (2004) that a snapshot observation usually provides a good estimate of the effective radius. Other ground-based results are discussed in Lamy et al. (2004) and are generally in good agreement with the above conclusion.

3.3. 17P/Holmes

17P was observed with the HST on 15 June 1999 at $r_h = 3.12$ AU inbound, $\Delta = 2.18$ AU and at a solar phase angle of 8°.5. The comet later reached perihelion on 11 May 2000 at $r_h = 2.17$ AU. The coma was canonical with $p = -1$. The nucleus was easily detected with excellent contrast thanks to a very faint coma (Fig. 5), and analysis of the two F675W images yields a nucleus radius of 1.71 ± 0.07 km. We also obtained a color index $(V - R) = 0.56 \pm 0.02$.

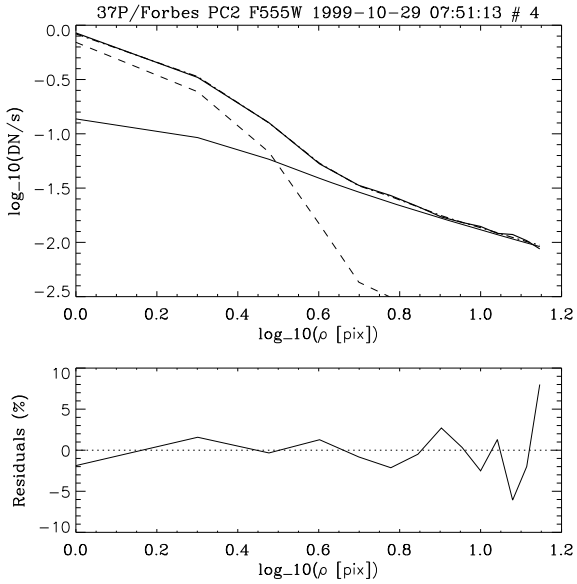

Fig. 6. Same as Fig. 2 for 37P/Forbes.

3.4. 37P/Forbes

37P was observed with the HST on 29 October 1999 when the comet was at $r_h = 2.27$ AU outbound, $\Delta = 1.39$ AU and at a solar phase angle of 14°.8. The comet had passed its perihelion on 4 May 1999 at $r_h = 1.45$ AU. The coma was canonical with $p = -1$. The nucleus was detected with good contrast, and the fits are excellent (Fig. 6). Analysis of the two F675W images yield an average value of the nucleus radius of 0.81 ± 0.04 km. We also obtained color indices $(V-R) = 0.29 \pm 0.03$ and $(R-I) = 0.66 \pm 0.06$.

37P was observed from the ground at $r_h = 3.59$ AU by Licandro et al. (2000). The stellar-like appearance of the image led them to conclude that they were seeing a bare nucleus, and they derived $r_n = 1.1$ km. Either a faint coma was still present in their images or we observed different cross-sections. Assuming that their and our circumstances correspond to the two extreme cross-sections, the spheroidal solution leads to $a = 1.38$ km, $b = 0.8$ km and $a/b = 1.73$.

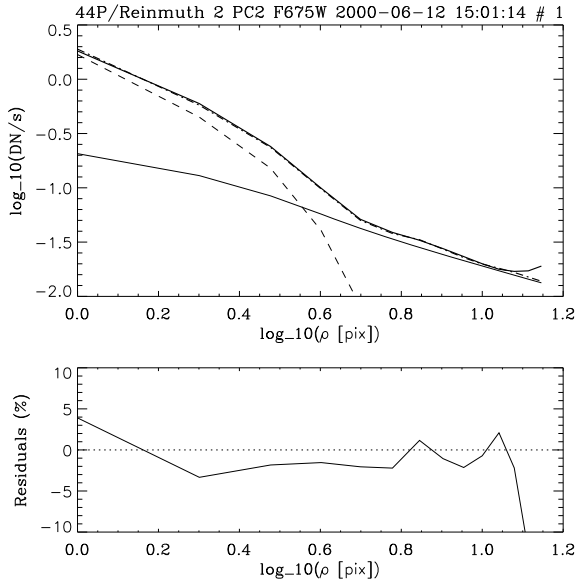

Fig. 7. Same as Fig. 2 for 44P/Reinmuth 2.

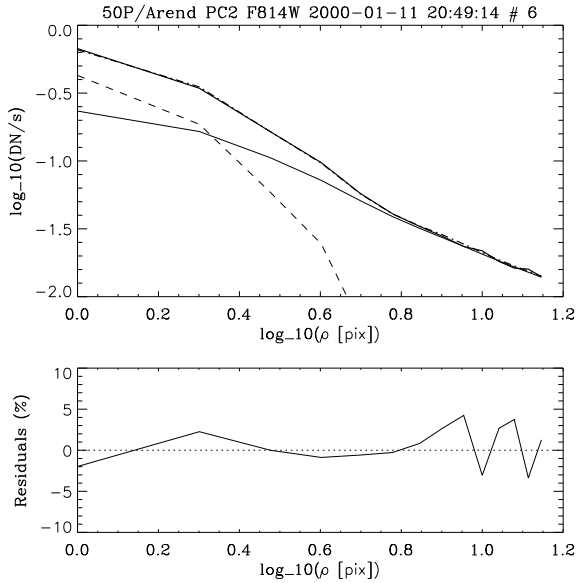

Fig. 8. Same as Fig. 2 for 50P/Arend.

3.5. 44P/Reinmuth 2

44P was observed with the HST on 12 June 2000 when the comet was at r_h = 2.73 AU inbound, Δ = 1.73 AU and at a solar phase angle of 5.°3. The comet was later at perihelion on 19 February 2001 at r_h = 1.89 AU. The coma was canonical with $p = -1$. The nucleus was detected with good contrast (Fig. 7). Analysis of the two F675W images yields an average value of the nucleus radius of 1.61 ± 0.07 km. The upper limit of 3.1 km reported by Lowry et al. (2003) is consistent with our result. We also obtained a color index $(V - R) = 0.62 \pm 0.08$.

3.6. 50P/Arend

50P was observed with the HST on 11 January 2000 when the comet was at r_h = 2.37 AU outbound, Δ = 1.47 AU and at a solar phase angle of 11.°8. The comet had passed its perihelion on 3 August 1999 at r_h = 1.92 AU. The nucleus was detected with moderate contrast, but the fits are excellent (Fig. 8) requiring, however, that different values of the power exponent p of the coma model be introduced for the different filters: $p = -1$ for F675W, $p = -1.15$ for F555W, and $p = -1.10$ for F814W. Analysis of the two F675W images yield an average value of the nucleus radius of 0.95 ± 0.03 km. Lowry & Weissman (2003) reported an upper limit of 5.16 km, consistent with our result. We also obtained color indices $(V-R) = 0.81 \pm 0.10$ and $(R-I) = 0.26 \pm 0.09$.

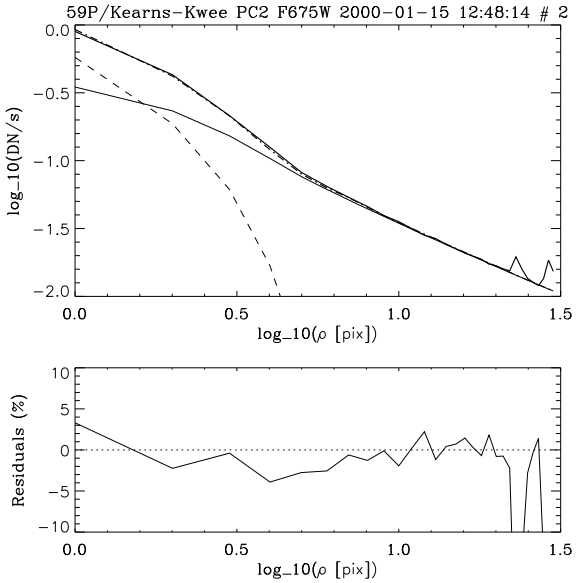

Fig. 9. Same as Fig. 2 for 59P/Kearns–Kwee.

3.7. 59P/Kearns–Kwee

59P was observed with the HST on 15 January 2000 when the comet was at r_h = 2.52 AU outbound, Δ = 1.54 AU and at a solar phase angle of 3.°3. The comet had passed perihelion on 16 September 1999 at r_h = 2.34 AU. The coma was canonical with $p = -1$ and very bright. The contrast of the nucleus over the coma is only 60% in the peak pixel, but the fits are nevertheless quite good (Fig. 9). Analysis of the two F675W images yielded an average value of the nucleus radius of 0.79 ± 0.03 km. At a phase angle of 3.°3, the apparent magnitude of the nucleus could be affected by an opposition effect. Assuming a phase function similar to that of 19P/Borrelly (Li et al. 2007), the correction for this effect would amount to ~0.04 mag (Lamy et al. 2007), and the radius of the nucleus would be reduced to ~0.76 km. We point out that it would be very difficult to detect such a small, very active nucleus from the ground. We obtained color indices $(V - R) = 0.62 \pm 0.07$ and $(R - I) = 0.27 \pm 0.08$.

3.8. 63P/Wild 1

63P was observed with the HST on 22 April 2000 when the comet was at r_h = 2.27 AU outbound, Δ = 1.30 AU and at a solar phase angle of 9.°2. The comet had passed perihelion on 27 December 1999 at r_h = 1.96 AU. The coma was canonical with $p = -1$ and quite faint. The nucleus was detected with excellent contrast, and the fits are almost perfect (Fig. 10). Analysis of the three F675W images yields an average value of the nucleus radius of 1.46 ± 0.03 km.

The non-detection by Lowry & Fitzsimmons (2001), which results in an upper limit $r_n \leq 0.6$ km, is therefore quite puzzling, unless we speculate that they observed the small cross-section

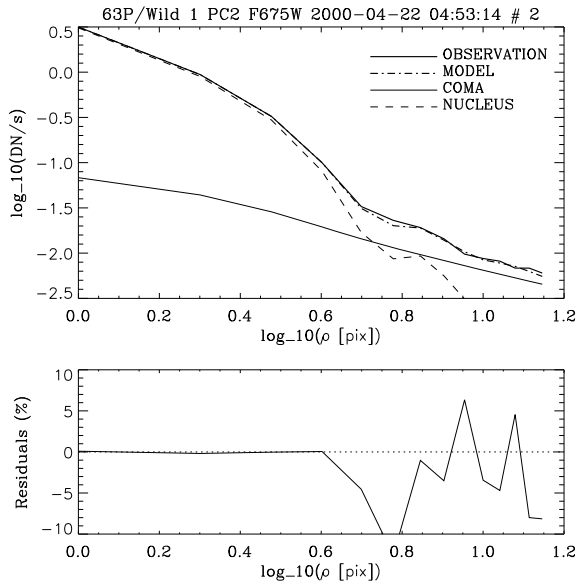

Fig. 10. Same as Fig. 2 for 63P/Wild 1.

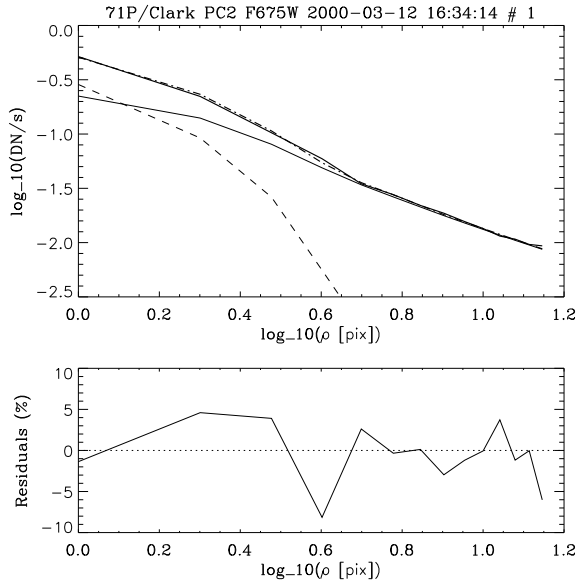

Fig. 11. Same as Fig. 2 for 71P/Clark.

of a highly-elongated spheroid with $a/b \gtrsim 8$, an incredibly large value. We obtained color indices $(V-R) = 0.50 \pm 0.05$ and $(R-I) = 0.42 \pm 0.04$.

3.9. 71P/Clark

71P was observed with the HST on 12 March 2000 at $r_h = 2.72$ AU inbound, $\Delta = 1.76$ AU and at a solar phase angle of 7°.5. The comet later passed perihelion on 2 December 2000 at $r_h = 1.56$ AU. The coma was quite bright and characterized by $p = -1.17$, thus deviating from steady state. The contrast of the nucleus is rather low (~25% in the peak pixel), by far the lowest of the present set of nuclei (Fig. 11). Analysis of the two F675W images yields an average value of the nucleus radius of 0.68 ± 0.04 km. This is consistent with the non-detection at $r_h = 4.4$ AU by Lowry & Fitzsimmons (2001), implying $r_n \leq 0.9$ km. The observations by Meech et al. (2004) at aphelion ($r_h = 4.67$ AU) yielded $r_n = 1.31 \pm 0.04$ km. A spheroid

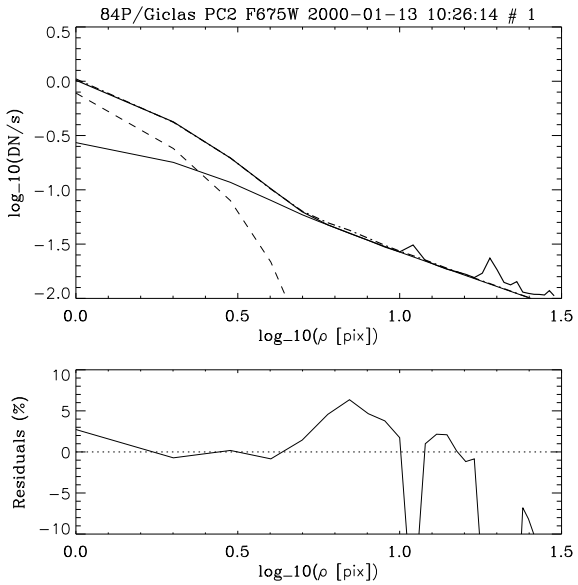

Fig. 12. Same as Fig. 2 for 84P/Giclas.

with $a = 2.13$ km and $b = 0.75$ km could reconcile the two extreme determinations within the error bars, but has a very large axis ratio, $a/b \geq 2.85$, and further requires that we observed nearly the smallest cross-section while Meech et al. (2004), the largest one. This nucleus certainly deserves further observations. We obtained a color index $(V-R) = 0.64 \pm 0.07$.

3.10. 84P/Giclas

84P was observed with the HST on 13 January 2000 when the comet was at $r_h = 2.21$ AU outbound, $\Delta = 1.37$ AU and at a solar phase angle of 16°.9. The comet had passed perihelion on 25 August 1999 at $r_h = 1.85$ AU. The coma was canonical with $p = -1$. The nucleus was detected with good contrast (a factor of ~3 in the peak pixel) and the fits are highly satisfactory (Fig. 12). Analysis of the two F675W images yields an average value of the nucleus radius of 0.90 ± 0.05 km. We obtained a color index $(V-R) = 0.32 \pm 0.03$.

3.11. 106P/Schuster

106P was observed with the HST on 18 October 1999 when the comet was at $r_h = 1.67$ AU inbound, $\Delta = 0.78$ AU and at a solar phase angle of 23°.00. The comet had passed perihelion on 16 December 1999 at $r_h = 1.56$ AU. The coma was canonical ($p = -1$) and very bright, but still the nucleus reaches a contrast factor of ~2.5 in the peak pixel (Fig. 13). Analysis of the two F675W images yields an average value of the nucleus radius of 0.94 ± 0.05 km. We obtained color indices $(B-V) = 1.01 \pm 0.06$, $(V-R) = 0.52 \pm 0.06$, $(R-I) = 0.45 \pm 0.06$.

3.12. 112P/Urata-Niijima

112P was recovered and observed with the HST on 8 September 1999 at $r_h = 2.30$ AU inbound, $\Delta = 1.50$ AU and at a solar phase angle of 19°.2. The comet later passed perihelion on 4 March 2000 at $r_h = 1.46$ AU. The comet appeared very faint with a weak canonical coma ($p = -1$). In spite of its low signal, the nucleus was easily detected with a huge contrast of a factor ~27 in the peak pixel, and the fits are excellent (Fig. 14).

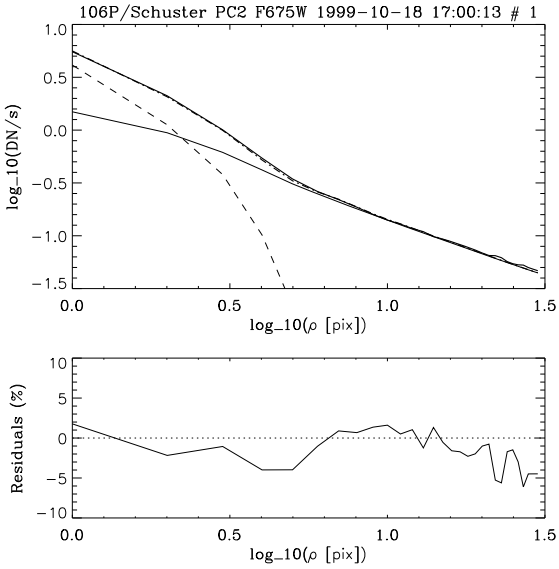

Fig. 13. Same as Fig. 2 for 106P/Schuster.

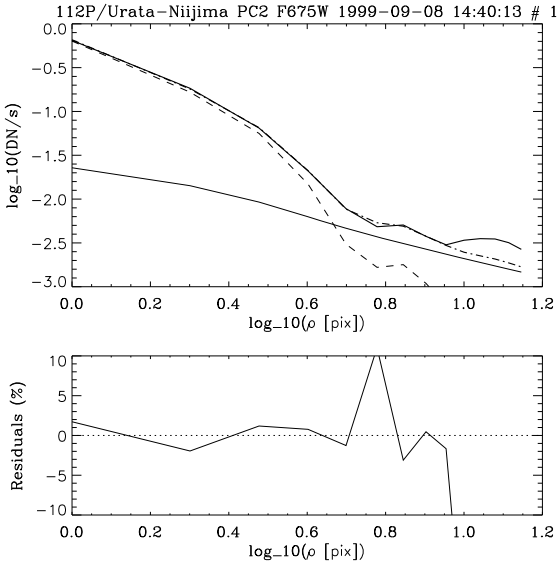

Fig. 14. Same as Fig. 2 for 112P/Urata–Niijima.

Analysis of the two F675W images yields an average value of the nucleus radius of 0.90 ± 0.05 km. We obtained a color index $(V - R) = 0.53 \pm 0.04$.

3.13. 114P/Wiseman-Skiff

114P was observed with the HST on 14 January 2000 when the comet was at $r_h = 1.57$ AU outbound, $\Delta = 0.84$ AU and at solar phase angle of 33°.2. The comet had passed perihelion on 11 January 2000, just a few days prior to our HST observations. The comet was consequently very bright and active, but its coma was canonical with $p = -1$. The nucleus was detected with good contrast (a factor ∼2.6), and the fits are excellent (Fig. 15). Analysis of the two F675W images yields an average value of the nucleus radius of 0.78 ± 0.05 km. We obtained color indices $(B - V) = 0.85 \pm 0.03$, $(V - R) = 0.46 \pm 0.02$ and $(R - I) = 0.54 \pm 0.02$.

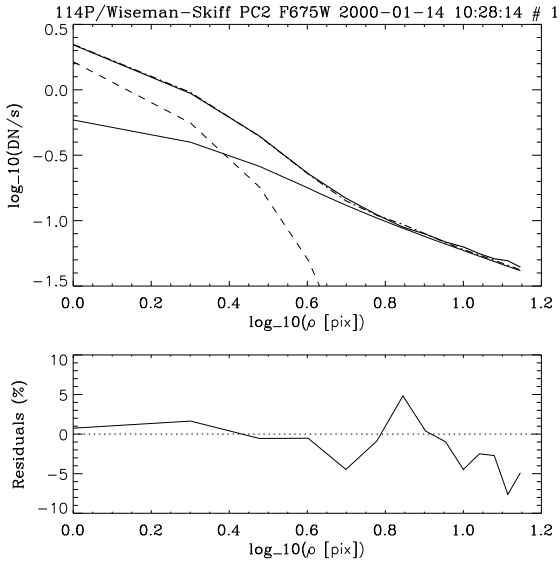

Fig. 15. Same as Fig. 2 for 114P/Wiseman–Skiff.

3.14. Colors of the nuclei

The various color indices derived from our measurements are reported in Table 4. The $(V - R)$ indices, to be compared with that of the Sun $(V - R)_\odot = 0.35$, range from slightly blue (37P) to ultrared (50P) and average to 0.52. Note that the nucleus of the recently captured comet 59P/Kearns-Kwee is quite red, but not the reddest. The reader is directed to the article by Lamy & Toth (2009) for an extended discussion of the colors of cometary nuclei in comparison with other primitive bodies of the solar system.

4. The properties of the comae

We now turn our attention to the comae of the 13 comets and present below results on the standard quantity $Af\rho$, which is proportional to the dust production rate and the dust reflectivity. These three quantities all involve the ratio $\mathsf{R} = F_{\rm coma}/F_\odot$, where $F_{\rm coma}$ and $F_\odot$ are respectively the radiance of the coma and that of the Sun (expressed for instance in erg s^{-1} cm^{-2} Å^{-1}) and averaged over a given spectral band. A convenient way to calculate R is to express it in terms of the signals measured on the images and expressed in DN/s:

$$\mathsf{R} = S_{\rm coma}/S_\odot \quad (8)$$

where $S_\odot$, the signal that would be produced by the Sun if observed by the HST WFPC2 in a given filter, is directly obtained from the transformation formulae of Holtzman et al. (1995) using the known magnitudes and color indices of the Sun.

4.1. Afρ

In order to quantify the activity of the observed cometary nuclei, we calculated the quantity $Af\rho$ (A'Hearn et al. 1984) by integrating the coma signal in a circular aperture with a diameter equivalent to 400 km at the distance of each comet using their fitted coma models. When the coma is in steady state ($p = -1$), the integrated coma signal $S_{\rm coma}$ is a constant which can be directly expressed in terms of k_c, the scaling factor of the coma model. When the coma is not in steady state, the integration is performed on the images of the coma model, and $S_{\rm coma}$

Table 5. Properties of the comae of the comets: $Af\rho$.

Comet	Year of perihelion	r_h (AU)	α (°)	λ or band (nm)	$Af\rho$ (cm)	Remark
4P/Faye	1991	1.78^I	15.5	524	380	AH+95
	1991	1.60^I	6.0	*R*	890	L+96
	1991	1.59^O	19.3	*R*	660	L+96
	2000	2.96^O	5.6	*R*	129 ± 6	This work
	2000	3.45^O	16.8	*R*	43.7 ± 3	LoW03
10P/Tempel 2	1988	1.78^I	20.3	524	20	AH+95
	1988	1.72^I	19.8	295	<40	FF91
	1988	1.72^I	20.3	684	17	AH+89
	1999	1.67^I	12.8	*R*	88 ± 4	This work
	1988	1.69^O	33.3	295	140	FF91
17P/Holmes	2000	3.12^I	8.5	*R*	20 ± 1	This work
37P/Forbes	1999	2.27^O	14.8	*R*	37 ± 2	This work
44P/Reinmuth 2	2001	4.73^I	10.3	*R*	≤2.3	LF+01
	2001	4.26^I	12.7	*R*	≤11.4	Lo+03
	2001	2.73^I	5.3	*R*	86 ± 1	This work
50P/Arend	1999	2.37^O	11.8	670	58 ± 3	This work
	1999	2.96^O	19.1	*R*	9.4 ± 2	LoW03
59P/Kearns–Kwee	1981	2.24^I	21.4	524	68	AH+95
	1999	2.52^O	3.3	*R*	112 ± 6	This work
63P/Wild 1	1999	2.27^O	9.2	*R*	14 ± 7	This work
71P/Clark	2000	4.40^I	8.2	*R*	≤2.2	LF+01
	2000	2.72^I	7.5	*R*	68 ± 1	This work
84P/Giclas	1999	2.21^O	16.9	*R*	60 ± 3	This work
106P/Schuster	1999	1.67^I	23.0	*R*	103 ± 5	This work
112P/Urata–Niijima	2000	2.30^I	19.2	*R*	5 ± 1	This work
114P/Wiseman–Skiff	2000	1.57^O	33.2	*R*	43 ± 2	This work

r_h: heliocentric distance.
I: inbound or *O*: outbound in the orbit.
α: solar phase angle.
λ: wavelength.
AH+89: A'Hearn et al. (1989).
AH+95: A'Hearn et al. (1995).
FF91: IUE observations by Feldman & Festou (1992).
L+96: Lamy et al. (1996).
LF01: Lowry & Fitzsimmons (2001).
Lo+03: Lowry et al. (2003).
LoW03: Lowry & Weissman (2003).

obviously depends upon the aperture size. Uncertainties on the $Af\rho$ values were calculated similarly to the errors calculated for the previously discussed nucleus fluxes. We display in Table 5 our results obtained with the F675W filter together with those already published in the literature. We selected this filter because it is very close to the *R* band often used by ground-based observers and because it is generally free of any major gas emission, and therefore relevant to the dust continuum. One should keep in mind that $Af\rho$, while being a proxy for the dust activity, does not directly provide the dust production rate Q_d. $Af\rho$ involves observational parameters, so that comparisons between various observations are generally not straightforward (even if the coma is in steady state, insuring that $Af\rho$ is independent of aperture size), a fact often overlooked by many cometary observers. This comes from the term *A*, the geometric albedo of the dust grains averaged over their size distribution, which is therefore a function of scattering angle (i.e., phase angle) and of wavelength via their optical properties (i.e., composition). Both parameters are therefore specified in Table 5. Finally, the various measurements were generally obtained at different apparitions and may reflect a variation in the intrinsic activity of a given comet. In spite of all these limitations, Table 5 indicates that the measurements are consistent with the expected behavior of $Af\rho$ with r_h. 4P/Faye appears as the strongest dust emitter in our data set. The variation of its $Af\rho$ with r_h is very coherent and part of the difference between our value of 129 cm at 2.96 AU outbound and that of Lowry & Weissman (2003) of 43.7 cm at 3.34 AU outbound may be ascribed to the different phase angles: at $\alpha = 5.6°$ (our observations), an opposition effect can artificially increase the albedo *A*. For 10P/Tempel 2, our value is about a factor 4 larger than those obtained by A'Hearn et al. (1989 and 1995) and Feldman & Festou (1992) at comparable heliocentric distances (1.7−1.8 AU) on the inbound leg, at rather similar phase angles, but at different apparitions. This possibly suggests a recent increase in the activity of this comet. Note the large value of 140 cm measured by Feldman & Festou (1992) at $r_h = 1.69$ AU outbound while it was <40 cm at $r_h = 1.72$ AU inbound. For 44P/Reinmuth 2, our value of 86 cm at $r_h = 2.73$ AU is consistent with the upper limits given by Lowry et al. (2003) and Lowry & Fitzsimmons (2001) much further away. Note here again that our small phase angle $\alpha = 5.3°$ likely tends to increase the $Af\rho$ value. For 50P/Arend, our value and that of Lowry & Weissman (2003) indicate that $Af\rho \propto r_h^{-8.3}$ in the range 2.4−3 AU outbound. Such a large power exponent is not uncommon and we note that a value of −8.89 was determined by A'Hearn et al. (1995) for 49P/Arend-Rigaux from their post-perihelion measurements. For 59P/Kearns–Kwee, our outbound value is certainly affected by a strong backscattering

Table 6. Properties of the comae of the comets: dust production rate and spectral reflectivity gradient.

Comet	r_h	Typical		Depleted		S'	Remark
		Q_{H_2O}	Q_d	Q_{H_2O}	Q_d	(%/kÅ)	
	(AU)	(mol s^{-1})	(kg s^{-1})	(mol s^{-1})	(kg s^{-1})		
4P/Faye	2.956^O	–	–	2.2×10^{26}	0.8		
	1.604^I	–	–	6.9×10^{27}*	127		L+96
	1.594^O	–	–	6.9×10^{27}*	153		L+96
10P/Tempel 2	1.669^I	1.8×10^{27}	2	–	–	12.4 ± 2.9	
17P/Holmes	3.116^I	1.4×10^{27}	4	4.4×10^{26}	1		
37P/Forbes	2.270^O	2.6×10^{27}	11	8.1×10^{26}	4	16.1 ± 3.0	
	2.06^I	$Q_d = 9.81$		NS85			
44P/Reinmuth 2	2.727^I	6.3×10^{27}	9	1.9×10^{27}	3		
50P/Arend	2.374^O	4.2×10^{27}	11	1.3×10^{27}	4	9.3 ± 3.3	
59P/Kearns–Kwee	2.516^O	9.7×10^{26}	5	–	–	10.5 ± 2.1	
	2.27^I	$Q_d = 24.75$		NS85			
63P/Wild 1	2.266^O	1.0×10^{27}	4	3.1×10^{26}	1	27.0 ± 3.3	
71P/Clark	2.715^I	4.9×10^{27}	13	1.5×10^{27}	5		
84P/Giclas	2.209^O	4.4×10^{27}	13	1.3×10^{27}	5		
106P/Schuster	1.666^I	7.5×10^{27}	20	2.3×10^{27}	8	12.1 ± 2.9	
112P/Urata–Niijima	2.296^I	3.6×10^{26}	4	1.1×10^{26}	1		
114P/Wiseman–Skiff	1.569^O	3.1×10^{27}	17	9.4×10^{26}	6	14.1 ± 2.9	

r_h: heliocentric distance.
I: inbound or O: outbound on the orbit.
Q_{H_2O}, Q_d: water and dust production rates.
*Derived from IUE measurements by Festou et al. (private communication).
S'[670, 792 nm]: normalized spectral reflectivity gradient.
L+96: Lamy et al. (1996).
NS85: Newburn & Spinrad (1985).

enhancement since $\alpha = 3.3°$. Correcting by a factor ~2 brings it more in line with the inbound measurement of A'Hearn et al. (1995). For 71P/Clark, our value of 68 cm at $r_h = 2.72$ AU and the upper limit of 2.2 cm at $r_h = 4.40$ AU (Lowry et al. 1999) both inbound are consistent.

4.2. Dust production rate

The determination of the dust production rate of the comet was performed using the method developed by Newburn & Spinrad (1985) and later re-formulated by Singh et al. (1992). The procedure is strictly identical to the one we applied to comet 4P/Faye (Lamy et al. 1996), 19P/Borrelly (Lamy et al. 1998b), 22P/Kopff (Lamy et al. 2002), 46P/Wirtanen (Lamy et al. 1998a). Assuming that the dust grains are roughly spherical, the mass release rate of dust expressed in g s^{-1} is given by

$$Q_d = \int_{a_0}^{a_m} \frac{4\pi}{3} a^3 \rho_d(a) f(a)\, da \qquad (9)$$

where $\rho_d(a)$ is the bulk density of grains of radius a and $f(a)$ is the size distribution function expressed in cm^{-1} s^{-1}:

$$f(a) = K\left(1 - a_0/a\right)^M \left(a_0/a\right)^N. \qquad (10)$$

In the above expression, $N = 4.2$ and M is given by

$$\log(M) = 1.13 + 0.62\ \log(r_h), \qquad (11)$$

where r_h is the heliocentric distance in (AU). The minimum radius of the dust grains is set to $a_0 = 10^{-5}$ cm while the maximum radius a_m corresponds to the largest grain that can be lifted from the nucleus by the gas drag forces. The normalization constant K expressed in cm^{-1} s^{-1} which appears in Eq. (10) is given by

$$K = \frac{2Ap(\lambda)}{\pi^2 s p_d(\lambda)} \left[\int_{a_0}^{a_m} \frac{a^2}{v_d(a)} \left(1 - \frac{a_0}{a}\right)^M \left(\frac{a_0}{a}\right)^N da \right]^{-1} \qquad (12)$$

where $Ap(\lambda)$ is the "observed" product of area and geometric albedo, $p_d(\lambda)$ is the geometric albedo of the dust grains irrespective of their size, $p_d(\lambda) = 0.04$, and s is the projected radius (in cm) of the nucleus-centered circular area in which the coma signal is measured. The velocity $v_d(a)$ of the dust grain of radius a was calculated using Eqs. (16)–(18) of Newburn & Spinrad (1985). These authors further presented an extensive discussion of the errors affecting the determination of Q_d.

We can assume that the activity is mostly driven by the sublimation of water ice for these ecliptic comets observed at heliocentric distances $r_h \leq 3$ AU. We must therefore estimate the water production rate of each comet at the heliocentric distance of the observations to calculate a_m. We checked several large data sets, namely Festou (1990), A'Hearn et al. (1995), Fink & Hicks (1996), Crovisier et al. (2002), and only found data for three of our comets in the second article, namely 4P/Faye, 10P/Tempel 2 and 59P/Kearns–Kwee. This article tabulates the OH production rates at specified heliocentric distances (Table III of A'Hearn et al. 1995). The variation of Q_{OH} with r_h can be obtained from their Table VII where they introduced two classes, "typical" or "depleted" comets, based on their abundance in carbon-chain species. 4P is classified as "depleted" while both 10P and 59P are "typical". The nature of the other 10 comets is unknown; therefore we calculated two values of Q_{OH} making use of two distinct empirical laws which relate Q_{OH} to $Af\rho$ (their Table VI) according to the above two classes "typical" and "depleted". Q_{H_2O} is derived from Q_{OH} using $Q_{H_2O} = 1.1\ Q_{OH}$ (Budzien et al. 1994).

Our results are presented in Table 6. For the comets for which we used the empirical relationships between Q_{OH} and $Af\rho$, there is typically a factor ~3 between the two values of Q_d coming from the two classes "typical" and "depleted" and up to a factor 4 for the three comets 17P, 63P and 112P, which have very low dust production rates. We feel that those factors give fair estimates of the uncertainties affecting Q_d. Table 6 includes the very

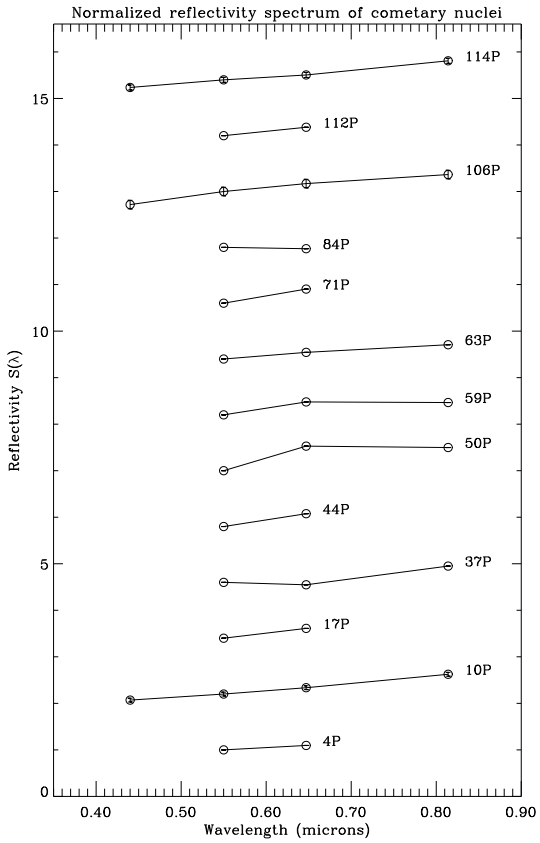

Fig. 16. Normalized reflectivity spectrum of the 13 cometary nuclei. When not shown, the error bars are much smaller than the size of the symbol. The spectra, normalized at 550 nm, are shifted for clarity.

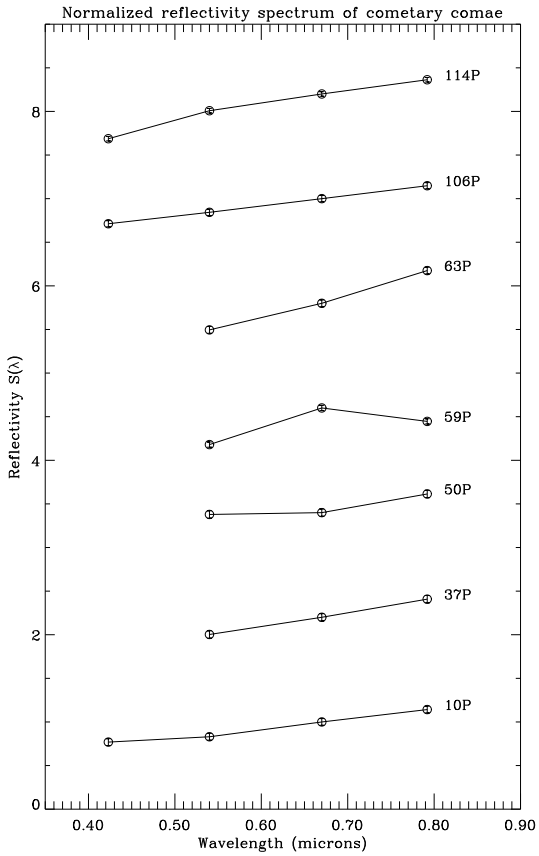

Fig. 17. Normalized reflectivity spectrum of the coma of 7 comets. When not shown, the error bars are much smaller than the size of the symbol. The spectra, normalized at 670 nm, are shifted for clarity.

scarce published determinations. For 4P/Faye, our past (Lamy et al. 1996) and present results lead to $Q_{\rm d} \propto r_{\rm h}^{-8.2}$, similar to what we found for the $Af\rho$ of 50P/Arend. For 37P/Forbes, applying the above power law to the value determined by Newburn & Spinrad (1985) leads to $Q_{\rm d} \simeq 4$ kg s^{-1} at $r_{\rm h} = 2.27$ AU inbound, similar to the value we obtained on the outbound leg in the "depleted" case. Applying the same scaling to the value determined by Newburn & Spinrad (1985) for 59P/Kearns–Kwee leads to $Q_{\rm d} \simeq 11$ kg s^{-1} at $r_{\rm h} = 2.52$ AU inbound while we found $Q_{\rm d} = 5$ kg s^{-1} at the same heliocentric distance but outbound and at a different apparition. Given that the accuracy of the dust production rates is no better than a factor 2 to 3, the above consistency between the past determinations and our recent results is a pleasant surprise.

4.3. Coma reflectivity

Figure 17 displays the normalized reflectivities of the comae calculated from the ratios $S_{\rm coma}/S_{\odot}$, further normalized at 670 nm, the effective wavelength of the F675W filter. The F439W filter may contain CN bands and the F555W filter may contain several C_2 bands while the other two filters, F675W and F814W, are probably free of any major gas emission and therefore provide reflectivity data that are representative of the dust continuum. Therefore, we only present the reflectivity of the seven comae for which we have data with these last two filters. In this spectral domain, all seven comae appear to reflect the properties of the dust and to be systematically redder than the Sun, a general rule for cometary dust (Jewitt & Meech 1986) with the exception of 59P/Kearns-Kwee. The normalized spectral reflectivity gradients $S'[670, 792\ nm]$ are listed in Table 6: they range from 9.3 ± 3.2 (50P/Arend) to 27 ± 3.3% per kÅ (63P/Wild 3) and average to 15.2 ± 2.3% per kÅ , excluding 59P/Kearns–Kwee. This latter comet is somewhat of a puzzle unless either the spectrum reflects the genuine, albeit unusual, properties of the dust or the F675W band is contaminated by an unusually bright gas emission (a possible candidate is NH_2). If we exclude the F675W data, the F555W and F814W measurements yield $S' = 10.6 \pm 2.1\%$ per kÅ, well within the range obtained from the other six comets. Our present results can be put in perspective with our past measurements obtained with the same instrumental configuration: $S'[670, 792\ \text{nm}] = 35 \pm 5\%$ per kÅ for the coma of comet 45/Honda-Mrkos-Pajdusakova (Lamy et al. 1999) and $S'[670, 792\ \text{nm}] = 17 \pm 3\%$ per kÅ for that of 22P/Kopff (Lamy et al. 2002). In a different spectral domain, the coma of 46P/Wirtanen had $S'[540, 670\ \text{nm}] = 8.3\%$ per kÅ, but probably a lower limit since the F555W band may have been contaminated by C_2 emissions (Lamy et al. 1998a).

5. Conclusions

Our main conclusions can be summarized as follows.

1. We successfully detected the nuclei of 13 ecliptic comets with the planetary camera 2 of the Hubble space telescope and with at least two filters (V and R), and up to four (B, V, R, I) for the brightest ones during cycle 8 (1999/2000). One HST orbit (~30 min of observational time) devoted to each comet did not permit measurement of secure light curves,

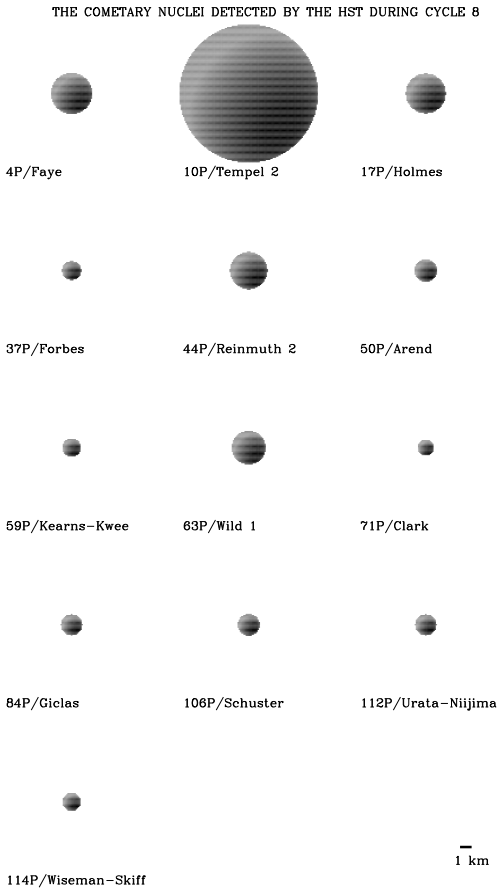

Fig. 18. A synthetic view of the 13 cometary nuclei detected with the HST during cycle 8 and idealized as spherical bodies.

and our "snapshot" observations yield effective radii which, on average, give excellent estimates of the effective radius of the equivalent spheres.

2. Assuming spherical nuclei with a geometric albedo of 0.04 for the R band (except 0.024 for 10P/Tempel 2 as measured independently), and a phase law of 0.04 mag/deg, we determined effective radii from the measured magnitudes. A synthetic view of our results is presented in Fig. 18, where we display their cross-sections assuming spherical nuclei. Eight of the thirteen nuclei (62%) have sub-kilometer radii: 37P/Forbes (0.81 km), 50P/Arend (0.95 km), 59P/Kearns–Kwee (0.79 km), 71P/Clark (0.68 km), 84P/Giclas (0.90 km), 106P/Schuster (0.94 km), 112P/Urata-Niijima (0.90 km), and 114P/Wiseman–Skiff (0.78 km). The average color of the nucleus of the observed 13 comets is $(V - R) = 0.52 \pm 0.04$, which is significantly redder than the Sun $[(V - R)_\odot = 0.36]$.
3. We determined the $Af\rho$ values for the comae of the 13 comets and found that they are generally consistent with past, ground-based measurements, keeping in mind that $Af\rho$ depends on several observational parameters: wavelength, phase angle, aperture size (if the coma is not in steady-state), and apparition. The dust production rates could be securely determined for three comets (4P/Faye, 10P/Tempel 2 and 59P/Kearns–Kwee) for which the OH production rates were independently measured. For the other ten comets, we used two different empirical relationships relating $Q_{\rm OH}$ and $Af\rho$ appropriate to the two classes "typical" and "depleted" introduced by A'Hearn et al. (1995). The resulting dust production rates differ by a factor 3 to 4, probably a fair estimate of the uncertainties. With the possible exception of 59P/Kearns–Kwee, the dust comae are redder than the Sun, and we determined an average value $S'[670, 792\,\text{nm}] = 15.2 \pm 2.3\%$ per kÅ for 6 comets.

Acknowledgements. I. Toth acknowledges supports from the bilateral French-Hungarian cooperation program, from the Université de Provence, from the Hungarian Academy of Sciences through grant No. 9871, and from the Hungarian State Research Foundation for Sciences (OTKA) through grant No. T025049. H. Weaver acknowledges financial support by NASA through grant HST–GO–8699.01–A from the Space Telescope Science Institute (STScI), which is operated by the Association of Universities for Research in Astronomy, Inc., under NASA contract NAS5-26555.

References

A'Hearn, M. F., Schleicher, D. G., Feldman, P. D., Millis, R. L., & Thompson, D. T. 1984, AJ, 89, 579
A'Hearn, M. F., Campins, H., Schleicher, D. G., & Millis, R. L. 1989, ApJ, 347, 1155
A'Hearn, M. F., Millis, R. L., Schleicher, D. G., Osip, D. J., & Birch, P. V. 1995, Icarus, 118, 223
Biretta, J. A., & 18 colleagues 1996, Wide Field and planetary camera 2 Instrument Handbook. Version 4.0, Space Telescope Science Institute, Baltimore
Budzien, S. A., Festou, M. C., & Feldman, P. D. 1994, Icarus, 107, 164
Crovisier, J., Colom, P., Gérard, E., Bockelée-Morvan, D., & Bourgois, G. 2002, A&A, 393, 1053
Festou, M. C. 1990, Comparative study of cometology from IUE observations (ESA, Evolution in Astrophysics: IUE Astronomy in the Era of New Space Missions, IUE Report), 3
Feldman, P. D., & Festou, M. C. 1992, IUE observations of periodic comets Tempel-2, Kopff and Tempel-1, in Proc. of Asteroids, Comets, Meteors III, 1991, ed. A. W. Harris, & E. L. G. Bowell, LPI, Houston, TX, 171
Fink, U., & Hicks, M. D. 1996, ApJ, 459, 729
Holtzman, J. A., Burrows, Ch. J., Casertano, S., et al. 1995, PASP, 107, 1065
Jewitt, D., & Meech, K. J. 1986, ApJ, 310, 937
Jewitt, D. C. 1991, Ap&SS, 167, 19
Jewitt, D. C., & Luu, J. 1989, AJ, 97, 1766
Keller, H. U. 1990, The nucleus, in Physics and Chemistry of Comets, ed. W. F. Huebner (Berlin: Springer-Verlag), 13
Krist, J. 1995, Simulation of HST PSF using Tiny TIM, in Astronomical Data Analysis Software and System IV, ed. R. A. Shaw, H. E. Payne, & J. J. E. Hayes (San Francisco: Astron. Soc. of the Pacific), ASP Conf. Ser., 77, 349
Lamy, P. L., & Toth, I. 1995, A&A, 293, L43
Lamy, P. L., & Toth, I. 2009, Icarus, 201, 674
Lamy, P. L., Toth, I., Grün, E., et al. 1996, Icarus, 119, 370
Lamy, P. L., Toth, I., Jorda, L., & Weaver, H. A. 1998a, A&A, 335, L25
Lamy, P. L., Toth, I., & Weaver, H. A. 1998b, A&A, 337, 945
Lamy, P. L., Toth, I., A'Hearn, M. F., & Weaver, H. A. 1999, Icarus, 140, 424
Lamy, P. L., Toth, I., Jorda, L., et al. 2002, Icarus, 156, 442
Lamy, P. L., Toth, I., Fernández, Y. R., & Weaver, H. A. 2004, The sizes, shapes, albedos, and colors of cometary nuclei, in Comets II, ed. M. Festou, H. U. Keller, & H. A. Weaver (Tucson, AZ: University of Arizona Press), 223
Lamy, P. L., Toth, I., Davidsson, B. J. R., et al. 2007, SSRv, 128, 23
Li, J.-Y., A'Hearn, M. F., McFadden, L. A., & Belton, M. J. S. 2007, Icarus, 188, 195
Licandro, J., Tancredi, G., Lindgren, M., Rickman, H., & Gil Hutton, R. 2000, Icarus, 147, 161
Lowry, S. C., & Fitzsimmons, A. 2001, A&A, 365, 204
Lowry, S. C., & Weissman, P. R. 2003, Icarus, 164, 492
Lowry, S. C., Fitzsimmons, A., Cartwright, I. M., & Williams, I. P. 1999, A&A, 349, 649
Lowry, S. C., Fitzsimmons, A., & Collander-Brown, S. 2003, A&A, 397, 329
Meech, K. J., Hainaut, O., & Marsden, B. G. 2004, Icarus, 170, 463
Newburn, R. L., Jr., & Spinrad, H. 1985, AJ, 90, 2591
Russell, H. N. 1916, ApJ, 43, 173
Singh, P. D., de Almeida, A. A., & Huebner, W. F. 1992, AJ, 104, 848
Weaver, H. A., & Lamy, P. L. 1999, Earth, Moon, & Planets, 79, 17